Carbohydrate Polymer Technologies and Applications 9 (2025) 100654

Contents lists available at ScienceDirect

Carbohydrate Polymer Technologies and Applications

journal homepage: www.sciencedirect.com/journal/carbohydrate-polymer-technologies-and-applications

Preparation of beta-cyclodextrin decorated magnetic lignin by citric acid cross-linker for water treatment

Arefe Moatamed Sabzevar [a,b], Ali Ahmadpour [a,b,*], Mahboube Ghahramaninezhad [a,b]

[a] Chemical Engineering Department, Faculty of Engineering, Ferdowsi University of Mashhad, P.O. Box 91779-48944, Mashhad, Iran
[b] Industrial Catalysts, Adsorbents, and Environment Lab., Oil and Gas Research Institute, Ferdowsi University of Mashhad, P.O. Box 91779-48974, Mashhad, Iran

ARTICLE INFO

Keywords:
Magnetic lignin
Cyclodextrin
Water treatment
Methylene blue
Citric acid

ABSTRACT

In this research, a straightforward method was used to prepare a multifunctional adsorbent for selective removal of cationic dyes. To synthesize this adsorbent, beta-cyclodextrin (beta-CD), due to the outstanding and unique structure of their caves, which have the appropriate size for trapping and adsorption of cationic dyes, was grafted onto magnetic lignin (ML) via citric acid cross-linker for the first time. Various techniques were applied to characterize magnetic adsorbent (beta-CD@ML), including Fourier transform infrared spectroscopy (FTIR), X-ray photoelectron spectroscopy (XPS), X-ray diffraction (XRD), and nitrogen adsorption-desorption analysis. To check the performance of the beta-CD@ML, the adsorption process was investigated to remove methylene blue from aqueous solutions. The best result for methylene blue removal was approximately 97 % under conditions of pH 7, beta-CD@ML dosage of 0.6 g L^{-1}, pollutant concentration of 20 mg L^{-1}, and time of 45 min, while the removal of methylene blue for magnetic lignin under the same conditions was 55 %. The appropriate model used in adsorption was the Langmuir isotherm, which showed a maximum adsorption capacity of 80 mg g^{-1}at 25 °C. The stability and reusability of beta-CD@ML adsorbent were also investigated, and the results showed a slight decrease in adsorption efficiency.

1. Introduction

Industrialization, uncontrolled urbanization, overuse of natural water resources, and population growth have significantly affected water quality (Rout et al., 2023). Wastewater treatment can recover water from industrial wastes (Saravanan et al., 2021). Dyes are necessary for manufacturing leather, paper, and mostly textiles because of their coloring properties. Unfortunately, they are discharged into aquatic environments without treatment and cause deterioration of water quality (Rius-Ayra et al., 2023). The presence of dyes, a large group of organic compounds, causes increasing environmental concerns (Sharma & Bhattacharya, 2017). Carcinogenesis, mutagenesis, and abnormalities or malfunctions of the brain, kidney, liver, and nervous system can occur in humans due to dye consumption (Saravanan et al., 2021). Methylene blue (MB) is now widely used as a dye for many purposes. The presence of MB dye in wastewater is a significant issue for humans and the environment (Mosoarca et al., 2022).

Urgent action is required to develop affordable, accessible, and eco-friendly technologies and materials for water pollutant removal and wastewater treatment (Waheed et al., 2021). Adsorption has become a common technique for purifying wastewater due to the simplicity of the process (Amiri-Khamakani et al., 2024), cost-effectiveness (Heravi et al., 2024), and the ability to recover the adsorbent (Zhou et al., 2018). Economical and environmentally friendly biosorbents can be easily modified to enhance their adsorption capacity (Osman et al., 2023). The use of cellulose, lignin, chitosan, and agricultural waste materials in the synthesis of green and biodegradable adsorbents has been considered for the removal of contaminants due to their natural abundance, economic, biocompatibility, and minimal environmental effects. Lignin is a natural and complex aromatic renewable biopolymer (Li et al., 2015). The presence of active sites in lignin molecules and its unique features, biocompatibility, renewability, affordability, and abundance allow it to efficiently adsorb various organic and inorganic pollutants from water (Ge & Li, 2018). Phenolic hydroxyl, carbonyl, and methoxy groups are functional groups in lignin. The reactivity of lignin in different chemical processes is directly influenced by the quantity of these functional groups (Katahira et al., 2018). The practical applicability of these adsorbents is significantly reduced due to their slow adsorption rate and limited adsorption capacity. Therefore, lignin can be modified to improve its performance as an adsorbent (Li et al., 2015).

* Corresponding author.
E-mail address: ahmadpour@um.ac.ir (A. Ahmadpour).

https://doi.org/10.1016/j.carpta.2024.100654

Available online 24 December 2024

Cyclodextrins are easily available, environmentally friendly, and renewable materials (Przybyla et al., 2020). The enzymatic decomposition of starch and sugar leads to the formation of supramolecular structures known as cyclodextrins (Farooq et al., 2023). They are generally composed of glucopyranoses linked by α−1,4 glycosidic linkages and constitute a unique class of cyclic oligosaccharides (Varan et al., 2017). Beta-cyclodextrin (beta-CD) has an outer surface that is hydrophilic and an inner cavity that is hydrophobic (Ghahramaninezhad & Ahmadpour, 2022). Numerous organic guest molecules can create guest-host complexes in a hydrophobic cavity if they are suitable in size and polarity. Hydrophilic groups of beta-CD lead to the dissolution of cyclodextrins in water and prevent their direct use to remove pollutants (Amran & Zaini, 2022). There are two ways to solve this problem: 1- creating grafting through different cross-linkers and 2- cross-linking through beta-CD cross-linkers (Verma et al., 2022). Various materials have been synthesized by mixing beta-CD with nanomaterials, including graphene oxide, carbon nanotubes, and metal-organic frameworks. However, preparing these nanomaterials is complex, expensive, and requires significant amounts of organic solvents. The selection of environmentally friendly materials is essential for the green preparation of beta-CD composites (Wei et al., 2023).

Li et al. (2023) synthesized a composite microsphere of lignin, cyclodextrin, and polyethyleneimine. Lignin stabilizes beta-CD in producing these microspheres, and epichlorohydrin acts as a cross-linker. The adsorption capacity of composite microspheres for 2,4-dichlorophenoxyacetic acid and bisphenol A were studied. The composite microspheres exhibited an excellent adsorption capacity compared to activated carbon, graphene oxide, MIL-53, and MIL-101-$(OH)_3$ (Wei et al., 2023). Petitjean et al. (2022) linked xanthan, locust bean gum, and chitosan with citric acid in an environmentally friendly process. The simultaneous incorporation of beta-CD and lignin enhances the adsorption capacity for hydrophobic pollutants. Based on the results, the xanthan/β-CD/lignin matrix is the most effective in adsorbing phenolic pollutants (Petitjean et al., 2022). The use of citric acid as a cross-linker has increased in recent years. Also, using citric acid to synthesize beta-CD polymer enables simultaneous adsorption (Liu et al., 2020). Green chemicals, such as citric acid, are essential to solve the issue of toxicity or minimize the use of toxic organic substances (Köse et al., 2022).

The first hypothesis of this study is that a straightforward method for modifying magnetic lignin (ML) with beta-CD via citric acid cross-linker can be developed to enhance the removal efficiency of MB from aqueous environments. Therefore, the present study aims to fabricate and ponder the properties of a magnetic biosorbent containing cyclodextrin as an eco-friendly and cheap modifying agent. Inexpensive, green, and readily available citric acid was used for grafting beta-CD onto ML to prepare a multifunctional biosorbent (beta-CD@ML). There is no precedent in the available literature on using citric acid to cross-link beta-CD onto magnetic lignin, and most of the cross-linkers used are toxic (Lu et al., 2019; Yang et al., 2016). Additionally, the synthesis method for this adsorbent is simple and short, utilizing only water as a solvent. The use of water as the solvent is an important feature because it reduces production costs compared to adsorbents that rely on toxic and expensive solvents. Also, the magnetic properties of this adsorbent facilitate easy separation in an aqueous environment, making it highly applicable for water treatment processes. The second hypothesis is that the removal of MB from the solution is driven by electrostatic interactions, complexation, hydrogen bonding, and π-π stacking between beta-CD@ML and MB.

The synthesis of beta-CD@ML was investigated to prove the hypotheses. The effect of contact time, beta-CD@ML dosage, pH and concentration of dye, and temperature on pollutant removal was fully investigated in this study. Additionally, experiments on adsorption kinetics, equilibrium isotherm, and thermodynamics were carried out to reveal the adsorption mechanism of MB on beta-CD@ML.

2. Materials and methods

2.1. Materials

All the substances were analytical grade and weren't treated further. Methylene blue, with an empirical formula of $C_{16}H_{18}ClN_3S{\cdot}3H_2O$ and a molecular mass of 373.8 g mol^{-1}, iron (III) chloride hexahydrate ($FeCl_3{\cdot}6H_2O$), iron (II) sulfate heptahydrate ($FeSO_4{\cdot}7H_2O$), potassium dihydrogen phosphate (KH_2PO_4), ammonia solution ($NH_3.H_2O$, 28 wt %), hydrochloric acid (HCl, 37 wt%), sodium hydroxide (NaOH), and absolute ethanol (CH_3CH_2OH), and citric acid (CA, $C_6H_8O_7$) were all purchased from Merck. Kraft lignin ($M_w \sim 10{,}000$ g mol^{-1}), and beta-cyclodextrin (beta-CD > 97 %) were obtained from Sigma-Aldrich. Deionized (DI) water with an electric resistance of 18.2 MΩ cm^{-1} from a Millipore Milli-Q water purification system was used to make working solutions.

2.2. Methods and instrumentations

X-ray diffraction (XRD) was used by (the Bruker D8 Advance) powder diffractometer using CuKα radiation (λ = 0.15406 nm) in the range of 2θ from 5 to 70° to evaluate the crystallinity of the structure. Thermo Nicolet Avatar 370 was used to conduct Fourier transform infrared spectroscopy (FTIR) and functional group analysis in the range of 400–4000 cm^{-1} using the KBr pellet technique. A field emission scanning electron microscope (FESEM, Tescan Mira3 FEG) with an EDS instrument was used to determine the surface morphology characteristics.

Specific surface area, according to the Brunauer-Emmett-Teller (BET) method, was gained using N_2 adsorption-desorption isotherms at 77 K on a BELSORP MINI II. The surface charge of the beta-CD@ML was measured using a Zeta potential analyzer (Wallis, France). X-ray photoelectron spectroscopy (XPS) measurements were conducted with BESTEC (Germany) with magnesium Kα X-ray radiation (1253.6 eV) to determine the percentage of chemical composition and elements on the surface of the samples. The adsorption effect of MB was analyzed using UV–visible spectroscopy (AnalyticJena-Spekol 1300.1) at a wavelength of λ_{max} = 664 nm. The magnetic properties of the adsorbent were recorded using a vibrating sample magnetometer (VSM, Magnetic Danesh Pajoh Inst., Iran). The contact angles of beta-CD@ML were measured using a manual setup to determine the surface wettability before and after MB adsorption.

2.3. Preparation of adsorbent

The proposed protocol for developing beta-CD@ML as a multifunctional adsorbent consists of two main steps. Each step is depicted in detail in Fig. 1.

2.3.1. Synthesis of magnetic lignin

Magnetic lignin, as a magnetic core of the adsorbent, was prepared using the modified method presented by Han et al. (Han et al., 2022). 2.1 g (7.5 mmol) of iron (II) sulfate heptahydrate and 3.0 g (11.1 mmol) of iron (III) chloride hexahydrate were dissolved in 50 mL of DI water and stirred for 40 min at 90 °C. Then, 1.0 g (0.1 mmol) of lignin was added to the mixture and stirred for 40 min. In the last step, 5 mL of ammonia (28 %) was added dropwise to this mixture under stirring at 80 °C for 1 h The terminating dark brown dispersion of the magnetic lignin was collected using an external magnet, washed with DI water, and dried overnight at 60 °C.

2.3.2. Synthesis of beta-CD@ML

beta-CD@ML was synthesized by the esterification-polycondensation process via CA and beta-CD on the surface of magnetic lignin. To do this, 0.1 g of ML with a certain amount of beta-CD, 0.4 g (2 mmol) of CA, and 0.24 g (1.7 mmol) of KH_2PO_4 as a catalyst were added in 15 mL of water simultaneously. After obtaining a uniform

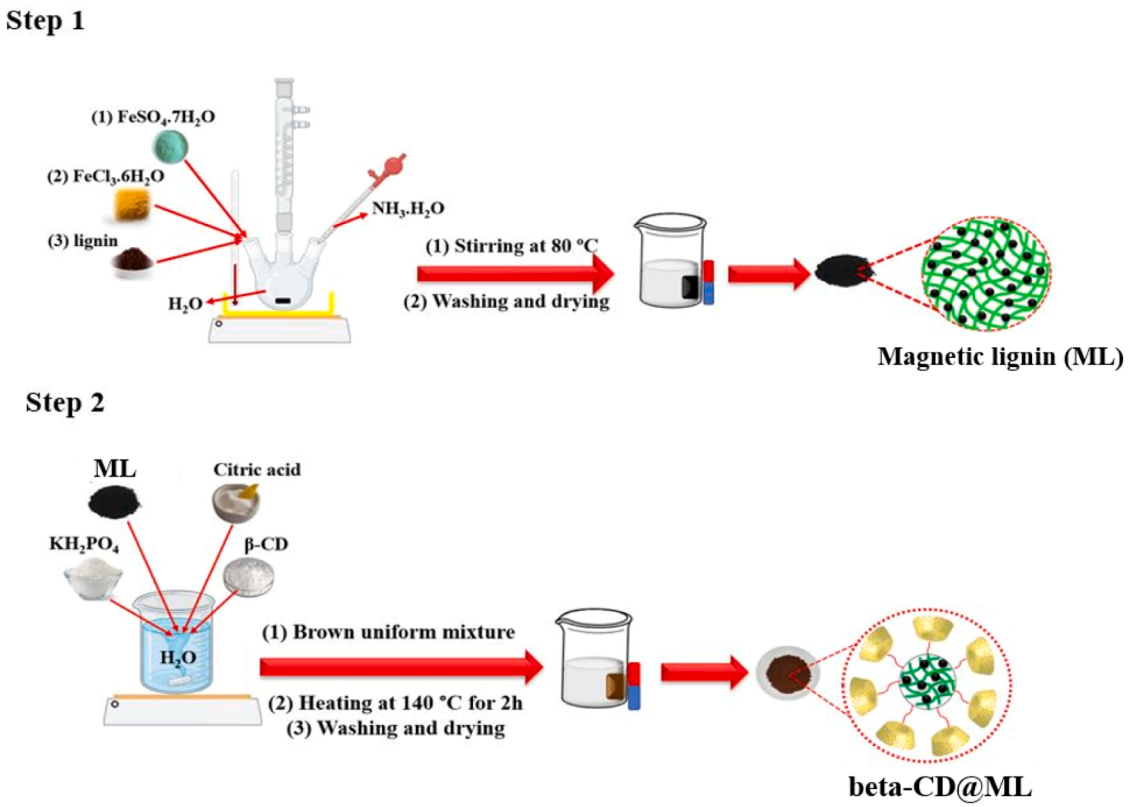

Fig. 1. Schematic of preparation of beta-CD@ML.

mixture, the mixture was transferred to a Petri dish to be heated at 140 °C for 2 h Then, the product obtained from this step was purified by soaking and washing several times with DI water after cooling. Ultimately, the desired magnetic adsorbent was dried at 60 °C overnight.

2.4. General method for the adsorption process

Practical experiments in the presence of beta-CD@ML for the removal of MB were set up and performed to thoroughly investigate how well the synthesized adsorbent performs during the adsorption process. In all experiments, beta-CD@ML was added to the MB dye solution in a volume of 25 mL. The effect of initial pH (3–11), temperature (25–45 °C), initial concentration of pollutant (5–150 mg L^{-1}), beta-CD@ML dosage (0.3–1.2 g L^{-1}), and contact time on the adsorption process were investigated separately. Moreover, 0.1 M NaOH or HCl was used to adjust the basic and acidic media, respectively. After a certain period of time, the adsorbent was collected using an external magnet. Then, the residual concentration of pollutant was monitored using a UV spectrophotometer. The R.E. and q_e were computed using Eqs. (1) and (2).

$$RE = \frac{(C_0 - C_t)}{C_0} \times 100 \tag{1}$$

$$q_e = \frac{(C_0 - C_e)V}{m} \tag{2}$$

where R.E. represents the efficiency of pollutant removal (%), C_0 and C_t (mg L^{-1}) denote the pollutant concentrations at the beginning and t times, respectively. The adsorption capacity of the beta-CD@ML (mg g^{-1}) and the residual concentration of the pollutant (mg L^{-1}) at equilibrium time are represented by q_e and C_e, respectively, m denotes the amount of beta-CD@ML (g), and V is the pollutant volume (L) (Yatimzade et al., 2024) .

2.5. Adsorption kinetics

Both pseudo-first-order (PFO) and pseudo-second-order (PSO) kinetic models were used to study the adsorption kinetics of MB on beta-CD@ML. These models are indicated by Eqs. (3) and (4), respectively. The parameters t (min) and q_t (mg g^{-1}) represent the contact time and the adsorption capacity at t time, respectively. The rate constants employed in PFO and PSO models are parameters k_1 (min^{-1}) and k_2 (g mg^{-1} min^{-1}), respectively (Yatimzade et al., 2024).

$$\text{Pseudo} - \text{first} - \text{order}: \ ln(q_e - q_t) = lnq_e - k_1 t \tag{3}$$

$$\text{Pseudo} - \text{second} - \text{order}: \ \frac{t}{q_t} = \frac{1}{k_2 q_e^2} + \frac{t}{q_e} \tag{4}$$

The model of Weber and Morris was used to study the diffusion mechanism between adsorbate molecules and adsorbents (Eq. (5)).

$$q_t = k_i t^{0.5} + C \tag{5}$$

where intercept is denoted by C, and the intraparticle diffusion rate constant is represented by k_i (mg $(g{\cdot}min^{0.5})^{-1}$) (Tanhaei et al., 2015).

2.6. Adsorption isotherms

Three widely known isotherms, Langmuir, Freundlich, and Temkin, were used to investigate the interaction between MB molecules and the beta-CD@ML surface. The linear forms of these isotherm models are provided by Eqs. (6) to (8):

$$\text{Langmuir}: \ \frac{1}{q_e} = \frac{1}{q_m} + \left(\frac{1}{K_L q_m}\right)\left(\frac{1}{C_e}\right) \tag{6}$$

$$\text{Freundlich}: \ lnq_e = lnK_f + \left(\frac{1}{n}\right) lnC_e \tag{7}$$

$$\text{Temkin}: \quad q_e = \frac{RT}{b_T} \ln a_T + \frac{RT}{b_T} \ln C_e \tag{8}$$

where q_m (mg g^{-1}), K_L (L mg^{-1}), and K_f ((mg g^{-1})(L mg^{-1})$^{1/n}$) are the maximum monolayer adsorption capacity, the Langmuir constant and the Freundlich constant, respectively. In the Freundlich model, n shows a dimensionless constant (Yatimzade et al., 2024).

The dimensionless parameter R_L of the Langmuir equation was determined by Eqs. (9):

$$R_L = \frac{1}{1 + K_L C_0} \tag{9}$$

In the Temkin model, R (J mol^{-1} K^{-1}) represents the universal gas constant. Parameters T (K), a_T (L g^{-1}), and b_T (J mol^{-1}) demonstrate the absolute temperature, equilibrium binding constant corresponding to the maximum binding energy, and the constant associated with the heat of adsorption, respectively (Ahmadpour et al., 2023).

2.7. Adsorption thermodynamics

By applying Eqs. (10), (11), and (12), the main thermodynamic parameters (△G°, △H°, and △S°) of MB adsorption on beta-CD@ML were calculated (Rahman & Raheem, 2023).

$$K = \frac{q_e * 1000}{C_e} \tag{10}$$

$$\Delta G^\circ = -RT \ln K \tag{11}$$

$$\ln K = -\frac{\Delta H^\circ}{RT} + \frac{\Delta S^\circ}{R} \tag{12}$$

where △G°, △H°, and △S° are the Gibbs free energy (J mol^{-1}), enthalpy (J mol^{-1}), and entropy (J mol^{-1} K^{-1}) changes, respectively. Parameter K is the equilibrium constant (Tanhaei et al., 2015).

3. Results and discussion

3.1. Synthesis of beta-CD@ML

Here, the amount of beta-cyclodextrin as a magnetic lignin surface modifier on adsorption capacity was investigated. According to Fig. 2 (A), the amount of MB adsorbed by the adsorbent enhances with the increase of beta-CD dosage compared to the unmodified magnetic lignin. This improvement can be attributed to the increase of adsorption sites and hybrid affinity between beta-CD@ML and MB, caused by hydrogen bonding and hydrophobic interaction between beta-cyclodextrin cavities and MB as dye contamination.

3.2. Characterization of synthesized beta-CD@ML

3.2.1. XRD analysis

As shown in Fig. 2(B), the X-ray diffraction pattern of beta-CD@ML

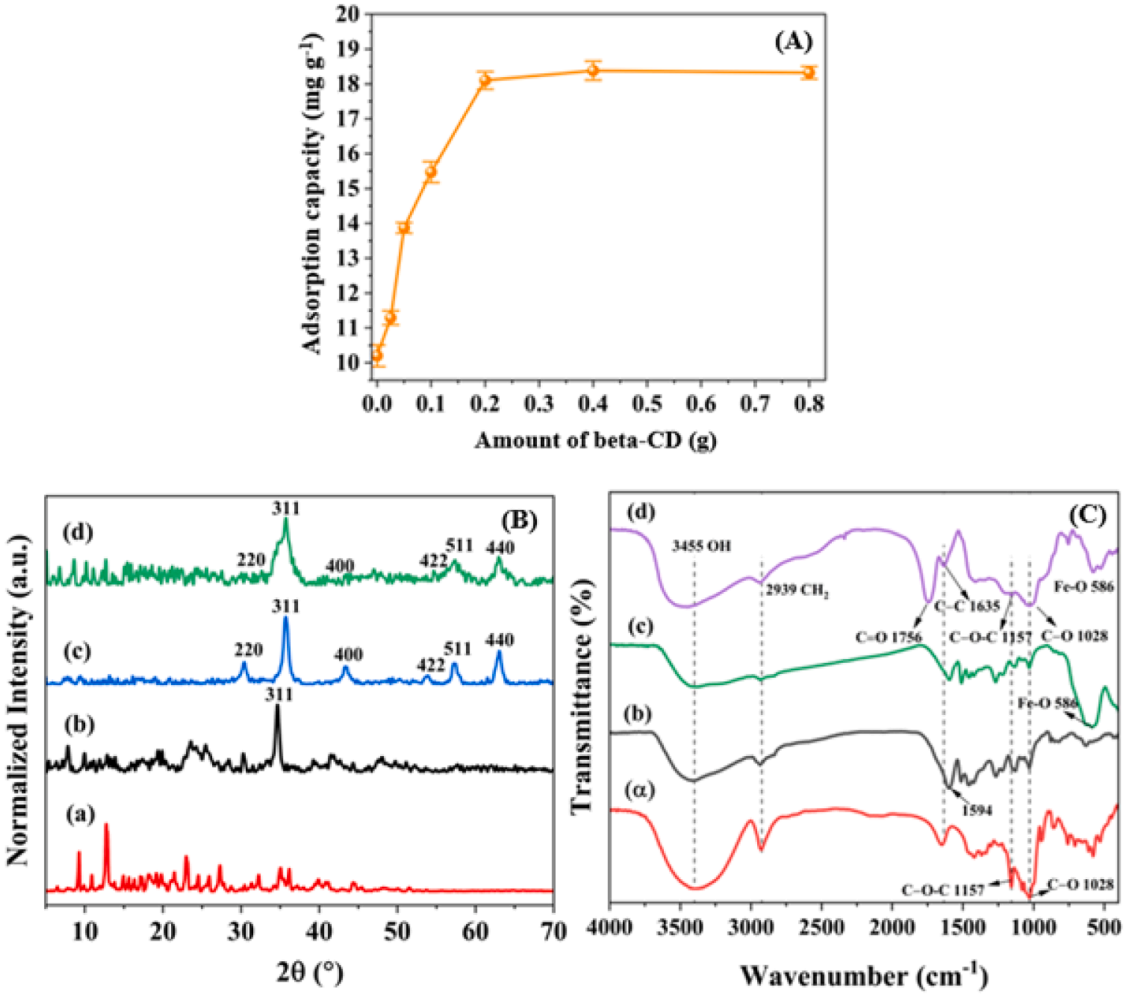

Fig. 2. (A) Effect of beta-CD on adsorption performance (C_0: 20 mg L^{-1}, pH: 7, beta-CD@ML dosage: 1 g L^{-1}, and time: 15 min). (B) XRD patterns and (C) Fourier transform infrared spectrum of (a) beta-CD, (b) lignin, (c) ML, and (d) beta-CD@ML.

was compared and analyzed with ML, beta-CD, and lignin. The presence of several distinct diffraction peaks in the spectrum of beta-CD at diffraction angles (2θ) of 9.25°, 12.76°, 22.98° and 27.41° indicates its high crystallinity (Qu et al., 2020). The presence of a peak around 35° in the pattern of (c) and (d) indicates lignin as the adsorbent base because such a peak is also present in pure lignin (M.J. Hasan et al., 2023). Diffraction peaks at 2θ of 30.12°, 35.90°, 43.31°, 53.90°, 57.44°, and 62.93° demonstrate the presence of Fe_3O_4 (Soares et al., 2019) in the structure of c and d. The XRD patterns of ML and beta-CD@ML show great similarities to Fe_3O_4, demonstrating that the crystalline structure of Fe_3O_4 remains intact. The intensity of lignin and the diffraction peak of beta-CD in ML and beta-CD@ML decrease, respectively. The XRD spectrum of beta-CD@ML shows additive noises due to the decrease in crystal size (Peng et al., 2021).

3.2.2. FTIR analysis

The FTIR spectrum (Fig. 2(C)) of ML shows peaks similar to the lignin structure. The distinct peak at 586 cm^{-1} in ML is related to the oscillation of the Fe-O bond in Fe_3O_4, indicating the successful loading of Fe_3O_4 into its structure (Han et al., 2022).

The presence of beta-CD is identified through a prominent peak at 1635 cm^{-1}. This peak is ascribed to the stretching vibrations of C—C bonds (Wei et al., 2023). Furthermore, the presence of ML is indicated by a distinct peak at 1594 cm^{-1}, corresponding to the vibrations of the benzene ring (M.J. Hasan et al., 2023). According to spectra (b) and (d), it can be stated that this peak overlaps with the significant peak at 1635 cm^{-1} observed in beta-CD@ML, which is most likely because of a cross-linking interaction between beta-CD and ML. In addition, the peaks at 1157 cm^{-1} and 1028 cm^{-1}, which are attributed to C—O-C and C—OH vibrations, respectively (Wei et al., 2023) in both spectra (a) and (c), are also present in spectra (d).

The appearance of a new peak at 1740 cm^{-1} in the FTIR spectrum of beta-CD@ML can be assigned to the stretching vibration of carboxyl/ester groups (C = O) (Zhou et al., 2018). This observation provides evidence of a successful esterification reaction, indicating chemical bonding between the components (Zhou et al., 2018). Furthermore, the broad bands at 3455 cm^{-1} are related to the stretching vibration of O—H bonds, while the bands at 2939 cm^{-1} correspond to the antisymmetric stretching vibration of -CH_2 groups (Wei et al., 2023). The presence of these distinct peaks confirms the effective grafting of beta-CD on ML and confirms the synthesis of beta-CD@ML.

3.2.3. FESEM analysis

FESEM images of ML and beta-CD@ML are shown in Fig. 3(a) and (b), respectively. The nanoparticles formed in Fig. 3(a) exhibit a spherical shape. The presence of aggregate structures suggests that the nanoparticles have a high surface energy, consistent with the findings of Soares et al. They reported that the nanostructure of Fe_3O_4@C (C: carbon base) tends to form agglomerate structures because the surface energy of nanoparticles is strong (Soares et al., 2019). Grafting of beta-CD (Fig. 3(b)) changed the size of the adsorbent particles. The average particle diameters for the ML and beta-CD@ML samples are 37.53 nm and 22.68 nm, respectively. However, the morphology of each particle remains visually unchanged and resembles the spherical geometry of ML particles.

EDS and the elemental maps (Fig. 4 and S1) show the presence of iron, carbon, and oxygen elements. The elemental maps demonstrate a uniform distribution of Fe on the surface of beta-CD@ML. In addition, elemental analysis was performed to confirm the change in the elemental composition of ML (carbon (20.19 %), oxygen (20.89 %), and iron (57.77 %)) after beta-CD grafting to form beta-CD@ML (carbon (40.30 %), oxygen (41.39 %), and Fe (14.10 %)). According to the EDS analysis results regarding the decrease of iron content in beta-CD@ML, the magnetic property is also greatly reduced, as shown in Fig. S4. These two results from elemental analysis and magnetic properties are consistent.

3.2.4. XPS

The XPS spectra of ML and beta-CD@ML are illustrated in Fig. 5(a). Peaks of 286.13 and 531.86 eV for C 1 s, and O 1 s, respectively (Wei et al., 2023), and 724.48 eV for Fe 2p (K. Hasan et al., 2023) are seen in ML and beta-CD@ML. Incorporation of beta-CD into ML increases the intensity of C 1 s and O 1 s peaks, resulting in higher carbon and oxygen content compared to ML (Table S1). However, the peak related to iron is significantly reduced, which is in agreement with the results of EDS and VSM. Fig. 5(b) shows the split peaks of C 1 s for beta-CD@ML. The peaks at 284.6, 286.2, and 288.06 eV are associated with the C—C/C = C/C—H bonds of cyclodextrin skeleton and lignin carbon ring structure, carbonyl bond of C = O and the O—C = O bond (Liu et al., 2022) of the ether bonds between lignin and beta-cyclodextrin, respectively. Two

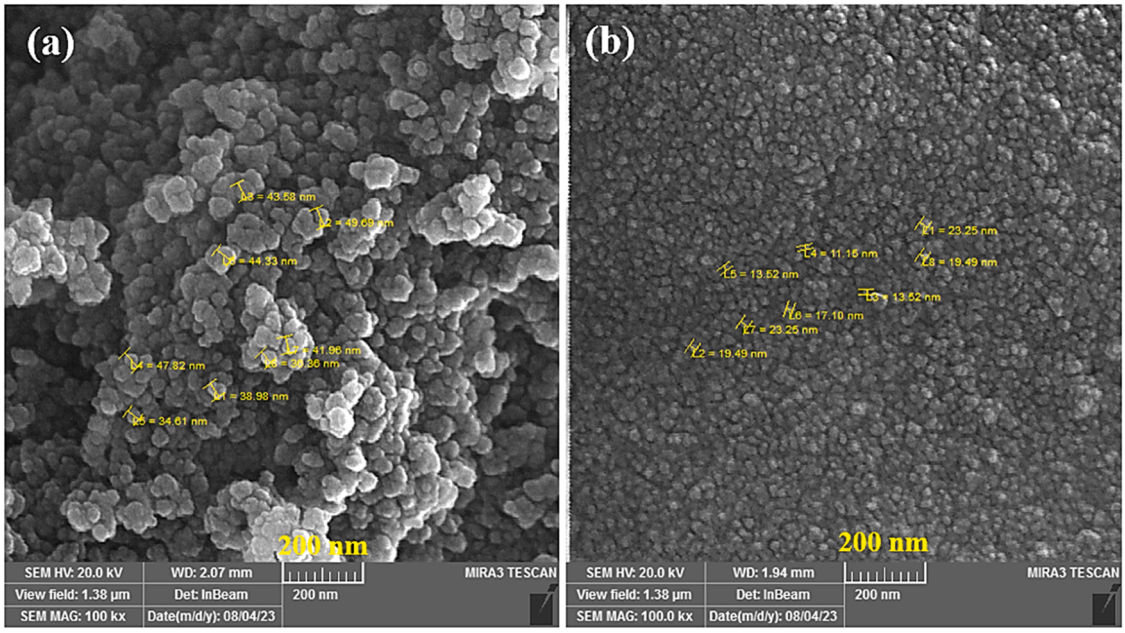

Fig. 3. FESEM images of (a) ML and (b) beta-CD@ML.

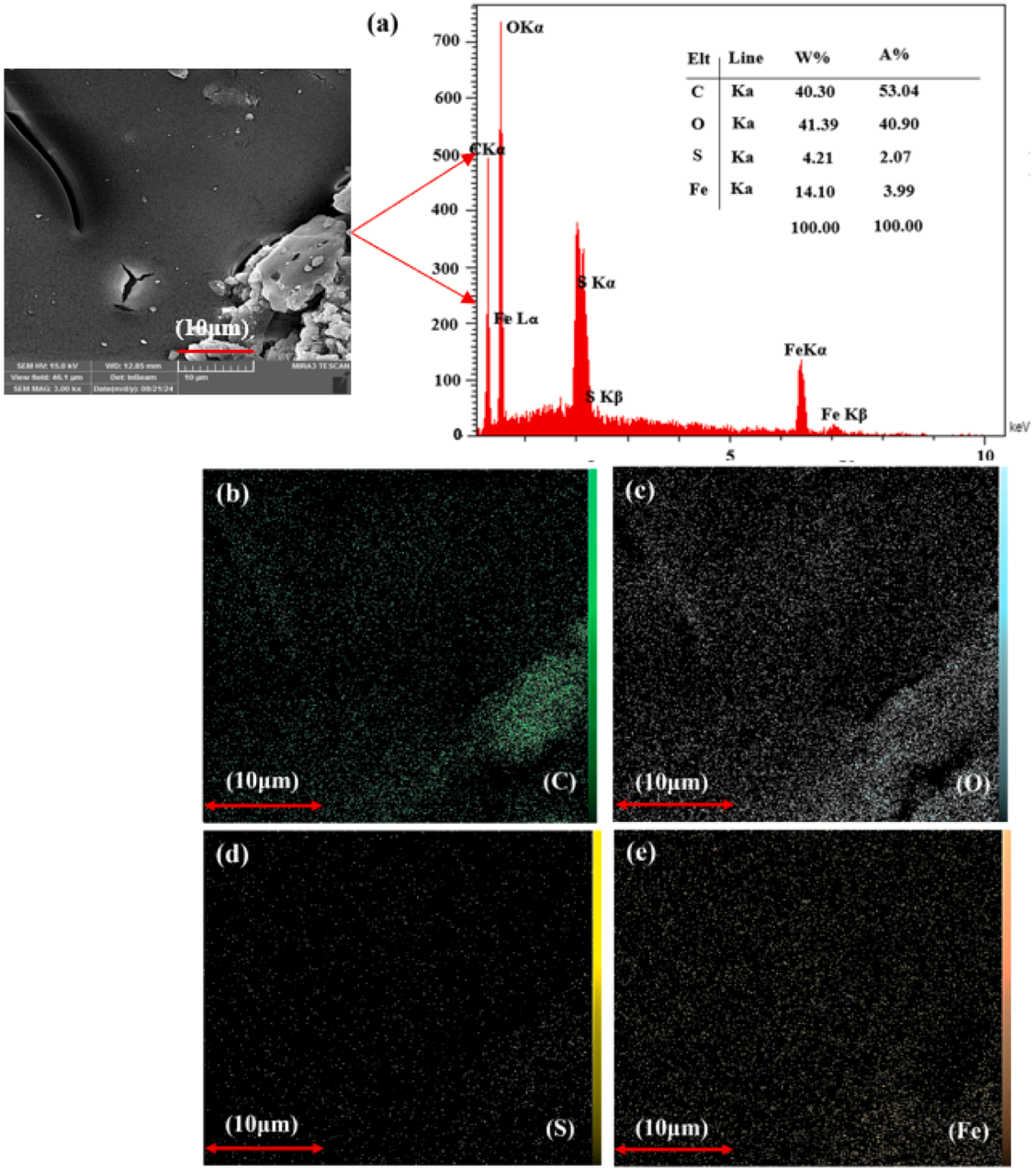

Fig. 4. EDS spectra and mapping analysis of beta-CD@ML.

peaks at 531.83 and 533.05 eV in the XPS curve of O 1 s (Fig. 5(c)) represent the C—O-C/O—H and C = O bonds, respectively (Zhang et al., 2023). Two peaks at 711.15 and 725.01 eV are observed in the Fe 2p scan of beta-CD@ML, as depicted in Fig. 5(d). The presence of Fe_3O_4 in beta-CD@ML is confirmed by the appearance of these two binding energy peaks, indicating Fe $2p_{3/2}$ and Fe $2p_{1/2}$ (Kohzadi & Soleiman-Beigi, 2021), respectively. The XPS spectra and split peaks of ML are shown in Fig. S2.

3.2.5. Nitrogen adsorption-desorption analysis

Nitrogen adsorption-desorption isotherm of ML (Fig. S3(a)) exhibits a type IV isotherm with H3 hysteresis, indicating a mesoporous structure. The desorption cycle of the isotherm, ranging from 0.3 to 0.97, is associated with capillary condensation in mesopores (Tanhaei et al., 2015). Gaps between nanoparticle agglomerates contribute to the porosity of the ML surface. These results are also observed in studies of Soares et al. with Fe_3O_4@C core-shell (Soares et al., 2019). The nitrogen adsorption-desorption isotherm of beta-CD@ML (Fig. S3(b)) also displays a type IV isotherm with H3 hysteresis. As noted in Table S2, after beta-CD grafting, there was a significant reduction in the pore volume and surface area of ML, which confirms the successful synthesis of beta-CD@ML. The SEM image (Fig. 3(b)) also confirms the low porosity in beta-CD@ML. The surface chemical property of the synthesized adsorbent, rather than its porous structure, plays a crucial role in MB adsorption.

3.2.6. Magnetic properties

The magnetic response of ML and beta-CD@ML was investigated using VSM measurements in a magnetic field of −15,000 to 15,000 Oe (Fig. S4). The saturation magnetization values obtained at room temperature were approximately 46.07 emu g^{-1} and 2.52 emu g^{-1} for ML and beta-CD@ML, respectively. The saturation magnetization value of beta-CD@ML was drastically lower than that of the ML. EDS mapping results also indicated an average iron content of 14.10 % for beta-

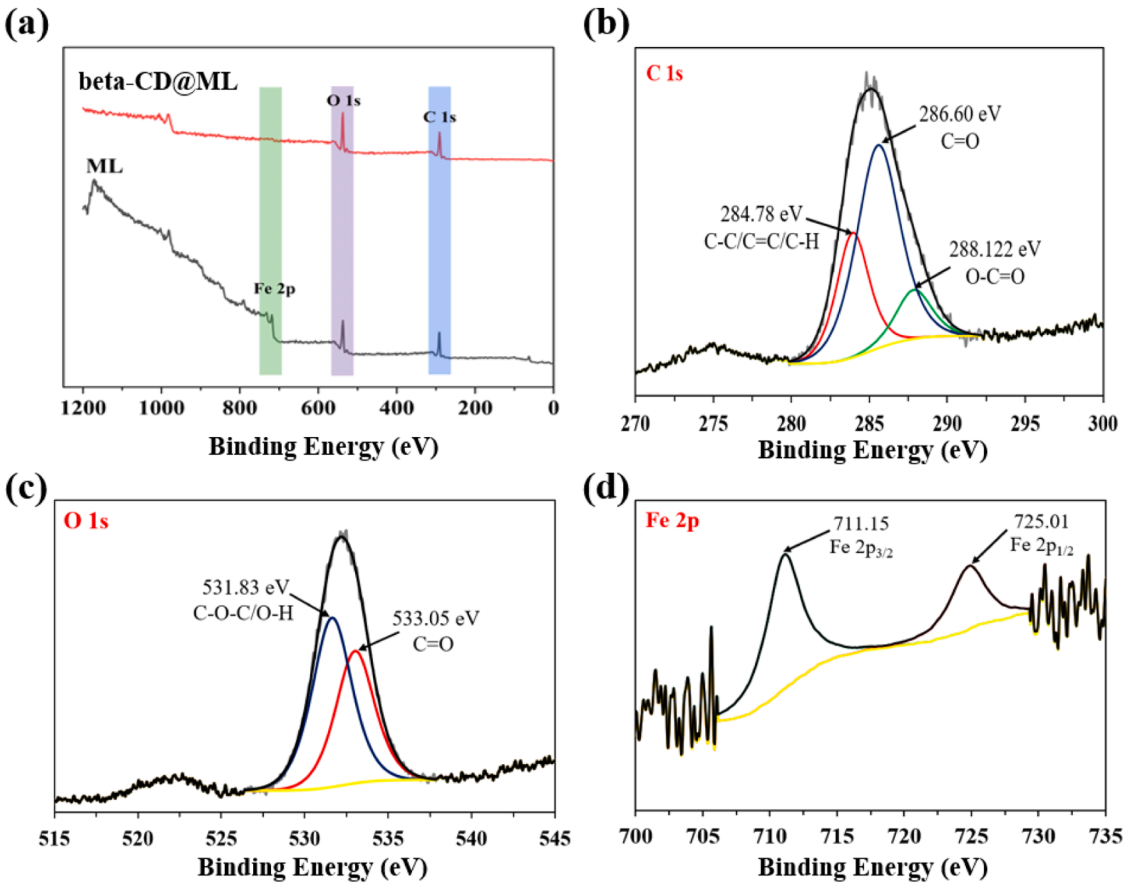

Fig. 5. (a) XPS spectra of ML and beta-CD@ML, (b, c, d) C 1 s, O 1 s, and Fe 2p XPS spectra of beta-CD@ML.

CD@ML. The significant reduction in magnetic properties can be attributed to the addition of non-magnetic beta-CD. This addition leads to a loss of magnetization and crystallinity in the ML, subsequently decreasing the magnetic permeability of the particles and quenching the magnetic moment. Similar findings have also been mentioned by Salazar et al. (Salazar et al., 2020). Despite the low amounts of VSM, recovery of adsorbent from the aqueous environment was easily achieved.

3.2.7. Contact angle

The contact angles of beta-CD@ML before and after MB adsorption were 68.1° and 57.3°, respectively, as shown in Fig. S5. The contact angle below 90° indicates the hydrophilic property of the adsorbent, which is explained by the existence of carboxyl (COOH) groups. The COOH groups, through hydrogen bonding, strongly attract water molecules (Lagiewka et al., 2023). The difference in interaction observed before and after adsorption is due to residual MB on the adsorbent surface. The presence of MB molecules helps to form adsorbent hydrogen bonds with water droplets and increases the hydrophilicity of the surfaces.

3.3. Adsorption properties of beta-CD@ML

3.3.1. Effect of initial pH

The zeta potential of beat-CD@ML at initial solution pH in the range of 3.0 to 11.0 is shown in Fig. 6(a). As illustrated, the zeta potential of beta-CD@ML varied from −15 to −28 mV at all measured pH conditions. This indicates that the surface of the beta-CD@ML adsorbent has a negative charge due to the deprotonation of carboxyl groups (Zhou et al., 2018). As observed in Fig. 6(b), the MB adsorption on beta-CD@ML was investigated under an MB solution of 20 mg L^{-1}, beta-CD@ML dosage of 0.6 g L^{-1}, and a contact time of 45 min at different pH.

Cationic dye molecules and H^+ ions compete for adsorption on the adsorbent's active sites at low pH levels. Therefore, the lowest amount of MB adsorption is expected under acidic conditions. Moreover, electrostatic repulsion between the adsorbent surface and the cationic dye molecules can also result from the adsorption of H^+ ions on the adsorbent surface (Khoshkho et al., 2021). As the pH increases, the H^+ion concentration in the solution decreases, causing MB to become protonated. This protonation increases the amount of dye adsorbed due to the electrostatic attractions (Lee et al., 2019) between beta-CD@ML and MB. The removal efficiency of MB in an acidic solution is almost 70 % at pH 3, while it increases to 97 % and 99 % at pH 7 and 11, respectively. Changes in the removal efficiency of MB at pH 7–11 are negligible.

3.3.2. Effect of adsorbent dosage

Efficient and cost-effective wastewater treatment relies on selecting the appropriate dosage of adsorbent (Khoshkho et al., 2021). The effect of beta-CD@ML dosage on MB removal was investigated by adding different amounts of adsorbent (0.3–1.2 g L^{-1}) to MB solution (20 mg L^{-1}) and shaking the mixture for 60 min. The results are presented in Fig. 6(c). The removal efficiency of MB shows an upward trend with an increase of beta-CD@ML dosage from 0.3 to 0.6 g L^{-1} due to the rise of empty and available adsorption sites (Khoshkho et al., 2021). The beta-CD@ML adsorbent exhibits a significant removal percentage (86 %) even at a low dosage (0.3 g L^{-1}). Beyond a dosage of 0.6 g L^{-1}, there is little change in the removal efficiency, indicating that equilibrium has been reached. Therefore, a dosage of 0.6 g L^{-1} is determined as the optimal value for the adsorbent.

3.3.3. Effect of contact time and adsorption kinetics

The adsorption kinetics of MB on beta-CD@ML at 20 and 40 mg L^{-1}

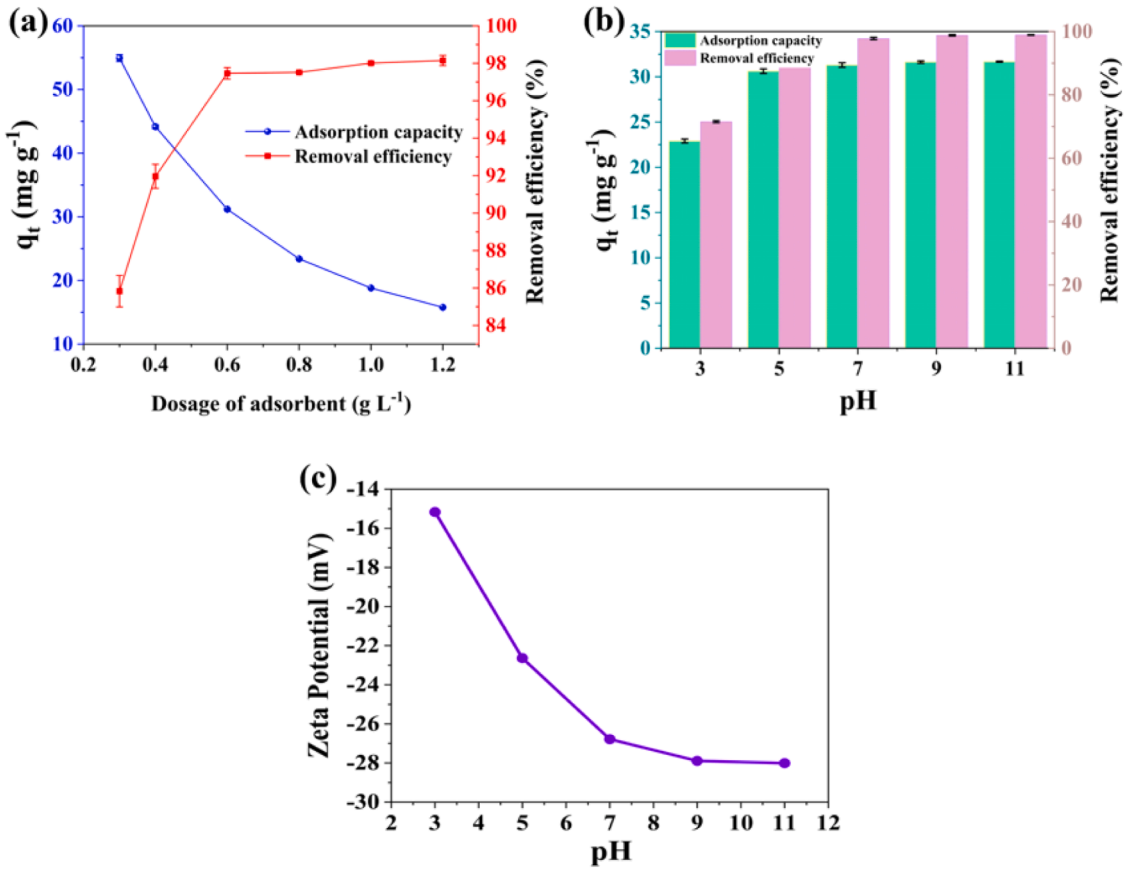

Fig. 6. (a) Zeta potential of beta-CD@ML, (b) the effect of pH of the solution, and (c) the effect of dosage of beta-CD@ML on the MB adsorption.

are depicted in Fig. 7(a). Fast adsorption and removal of 72 % MB occurs in the first 15 min for $C_0 = 20$ mg L^{-1} and within 45 min for $C_0 = 40$ mg L^{-1}. Then, a slower phase starts after 30 min for $C_0 = 20$ mg L^{-1} and 60 min for $C_0 = 40$ mg L^{-1} until equilibrium is reached, where more than 90 % of the dye is removed. The fast adsorption can be associated with the many vacant surface sites in the beta-CD@ML adsorbent. As the adsorption process progresses, the adsorption rate decreases steadily until it reaches equilibrium, likely due to the slow diffusion of MB molecules into the bulk (Khoshkho et al., 2021) of beta-CD@ML. Higher initial pollutant concentrations (40 mg L^{-1}) also increase adsorption, indicating a stronger driving force for mass diffusion (Wei et al., 2023).

To understand the adsorption mechanism, experimental data were evaluated using PFO and PSO (Fig. 7(b), and Table S3), as well as intraparticle diffusion models (Fig. 7(c) and Table S4). In the PSO model, q_e shows a significant difference between experimental ($q_{e,\ exp}$) and theoretical ($q_{e,\ cal}$) data. Furthermore, the correlation coefficient (R^2) is low. The PFO model fits a high R^2 value well and perfectly aligns the theoretical q_e values with the experimental values. These findings emphasize the significance of physical interaction in the adsorption of methylene blue on beta-CD@ML.

Analysis of the fitting results (Fig. 7(c)) indicates that two processes control the adsorption of methylene blue on beta-CD@ML. The first step in external diffusion is the transfer of methylene blue molecules from the bulk solution to the beta-CD@ML surface. Then, MB molecules migrate from the surface into the adsorbent through an internal diffusion process until adsorption equilibrium is reached. The active sites on the surface of the beta-CD@ML, combined with many MB molecules in the bulk solution, lead to higher external diffusion coefficients ($k_{i1} > k_{i2}$). This indicates a faster external diffusion process in the initial stage. However, the increased boundary thickness in the second stage ($c_{i2} > c_{i1}$) signifies greater resistance to intraparticle diffusion, leading to a slower intraparticle diffusion rate compared to external diffusion (Wei et al., 2023). Furthermore, N_2 adsorption-desorption isotherms indicate that beta-CD@ML has limited pores and channels that make it difficult for pollutants to penetrate into the adsorbent. The adsorption of MB on beta-CD@ML appears to involve a complex process, including intraparticle diffusion and physical mechanisms.

3.3.4. *Effect of concentration and adsorption isotherms*

The effects of initial MB concentration on adsorption phenomena were investigated using 0.6 g L^{-1} of beta-CD@ML at various adsorbate concentrations (5–150 mg L^{-1}) and temperatures (298, 308, and 318 K). As shown in Fig. 7(d), the change in adsorption capacity (q_e) is a function of equilibrium concentration (C_e). As the concentration of the MB solution increases, the adsorption capacity of beta-CD@ML gradually increases until it reaches maximum adsorption capacity at equilibrium. The abundance of adsorption sites in beta-CD@ML leads to a considerable rise in adsorption at lower concentrations and enhances the adsorption capacity for MB molecules (Wei et al., 2023). Moreover, the increase in temperature led to more adsorption of MB on beta-CD@ML, as shown in Fig. 7(d), because the increased mobility of MB molecules in solution at higher temperatures leads to an increase of mass transfer and MB adsorption on beta-CD@ML (Wu et al., 2021).

Typical isotherms for adsorption in an aqueous phase, such as Langmuir, Freundlich, and Temkin, were employed to fit the adsorption data, and the fitting parameters are presented in Table S5. There is excellent agreement between the experimental data and the Langmuir isotherm model, which is indicated by the high values of R^2 (> 0.999). This model demonstrates that monolayer adsorption is the primary mechanism of adsorption. Furthermore, all Freundlich constant n values were greater than 2, revealing that the adsorption process is favorable (Ahmadpour et al., 2023). The results show that the adsorbent surface is homogenous, and monolayer adsorption occurs. Based on the Langmuir isotherm, beta-CD@ML showed the theoretical saturation adsorption

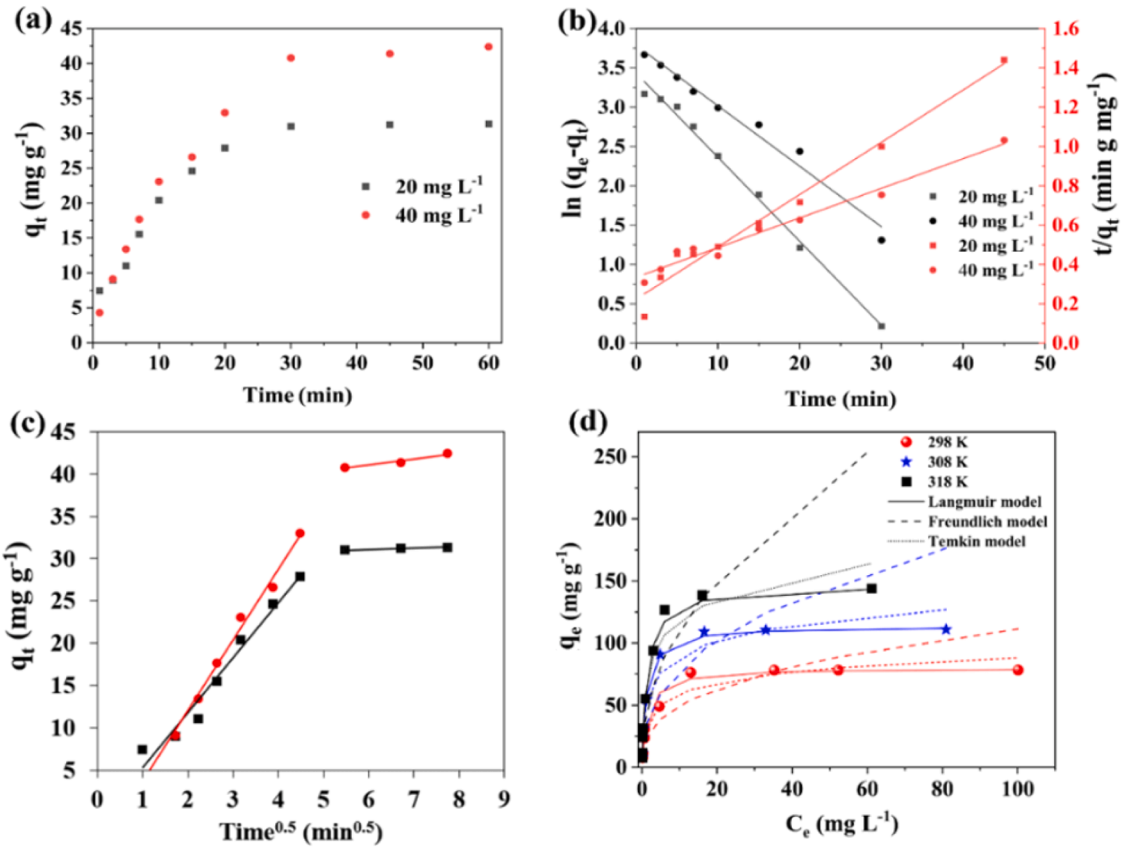

Fig. 7. (a) Adsorption kinetics MB on beta-CD@ML, (b) kinetics fitting results of PFO and PSO models, (c) results of intraparticle diffusion model, and (d) isotherms fitting results.

capacity of 80–147.06 mg g^{-1} for MB at 298–318 K, respectively. The values of b_T obtained from the Temkin model are in the range of 0.1981–0.1061 kJ mol^{-1}, corresponding to the heat of adsorption. The values of the separation factor constant R_L were used to evaluate the suitability of the beta-CD@ML for MB adsorption. The R_L values observed in this study were 0.3 to 0.96, which, according to Table S5, displayed the favorable adsorption of MB on beta-CD@ML.

3.3.5. *Adsorption thermodynamics*

The adsorption capacity of MB on beta-CD@ML increases from 28.09 to 28.46 and 28.54 mg g^{-1} as the temperature rises from 298 to 308 and 318 K, respectively (Fig. S6(a)). With rising temperatures, the solution's viscosity reduces, causing more collisions between beta-CD@ML and MB molecules, enhancing adsorption.

The results of fitting the adsorption data with the R^2 value of 0.98 to the Van't Hoff equation (Eq. (12)) are shown in Fig. S6(b). The slope and intercept of Fig. S6(b) were used to calculate the values of ΔH° and ΔS°. $\triangle H^\circ$ determines endothermic or exothermic nature, and $\triangle S^\circ$ describes the molecular movement (Khoshkho et al., 2021).

Table S6 displays the thermodynamic parameters of adsorption. Negative ΔG° values were observed for the MB adsorption on the beta-CD@ML at 298, 308, and 318 K, in the range of 26.366 to 27.374 and 28.639 kJ mol^{-1}.

Positive $\triangle H^\circ$ values (36,079.43 J mol^{-1}) demonstrate that MB adsorption on beta-CD@ML is endothermic. The adsorption process of MB using beta-CD@ML leads to an increase in the degree of freedom at the solid-solution interface, as indicated by the positive values of $\triangle S^\circ$ (209.38 J mol^{-1} K^{-1}) (Tang et al., 2019). The reason for the rise in entropy is the decrease in the number of water molecules surrounding the pollutants due to MB adsorption on the surface of beta-CD@ML. When MB molecules are adsorbed on the surface, the reorientation of water molecules around the adsorbent gain more entropy than the entropy lost because of pollutant adsorption. Consequently, the degree of freedom of the system increases (Wei et al., 2023).

3.4. *Selectivity studies*

Fig. S7(a) presents the removal efficiency of MB and Methyl Orange (MO) in separate solutions with a concentration of 20 mg L^{-1} and an equivalent mixture. The removal efficiency of MB and MO in a single-component solution was 97 % and 5 %, respectively, and in the two-component mixture, MB decreased from 97 % to 95 %. In contrast, there was no significant change in MO compared to the previous one-component mixture. The presence of carboxyl groups leads to electrostatic repulsion and makes acidic dyes such as MO less desirable. Cationic dyes such as MB, which contain a positive ionizable group of nitrogen or sulfur, can be efficiently removed by beta-CD@ML in binary mixtures. The 2 % decrease in removal efficiency was observed in the two-component combination of MB and MO. The electron density in the cationic groups can be altered when the two dyes interact to form the MB-MO complex. The interaction between the dyes, leading to the formation of the MB-MO complex, has implications for adsorption behavior. The potential alteration in the structure of MB may affect the efficiency of its removal process.

Similar results in previous studies involving CD-based polymeric adsorbents, particularly those containing a carboxylic group, are consistent with the idea that the interaction between different dyes and the influence of complex formation play a crucial role in the adsorption behavior (Zhou et al., 2018). Selectivity studies showed that beta-CD@ML is highly selective, making it a promising approach to removing other positively charged groups. The removal efficiency of methylene blue, crystal violet (CV), and malachite green (MG) on

beta-CD@ML is demonstrated in Fig. S7(b). The removal efficiencies for CV and MG are 73 % and 65 %, respectively, indicating that their similar molecular structures contribute to these comparable values. An image of the removal of MB cationic dye in a two-component solution consisting of MB and MO is presented in Fig. S7(c).

3.5. Effect of ionic strength

Adsorption processes can also be influenced by salinity. An aqueous solution with varying ionic strength directly impacts the adsorption in the aqueous phase. In the present study, NaCl was added to MB solutions to investigate the effects of salinity or ionic strength. Concentrations in the range of 0.001 to 0.5 M were used to prepare NaCl solution. As shown in Fig. 8(a), the removal efficiency of methylene blue decreased by 71 % at the 0.5 M NaCl concentration. Due to the electrostatic interaction, the positively charged cations MB and Na^+ form a strong bond with the carboxylate anion present in the adsorbent. The presence of Na^+ at higher concentrations blocks the adsorbent binding sites and leads to competition with MB. Jacob et al. also reported similar findings (Lagiewka et al., 2023).

3.6. Reusability

The adsorption process faces two major challenges: the capacity of the adsorbent for regeneration and its cost. An essential component for determining the adsorbent's performance is its regenerative ability. A selective combination of ethanol/0.1 M hydrochloric acid in a ratio of 3:1 proved to be the best solution for regeneration (Lagiewka et al., 2023). 0.6 g L^{-1} of beta-CD@ML was mixed with 20 mg L^{-1} MB solutions for 45 min at pH 7. Subsequently, the adsorbent was separated using an external magnet and mixed with 25 mL of regenerating mixture of ethanol/0.1 M hydrochloric acid for 45 min. After the desorption process, the adsorbent is recovered. Then, it was washed and dried to regenerate beta-CD@ML (dried at 50 °C for 12 h). These adsorption and desorption cycles were carried out five times.

The excellent reusability of beta-CD@ML in MB adsorption is evident in Fig. 8(b), where the removal efficiency of MB changes slightly during five adsorption-desorption cycles. A phase transition is catalyzed by HCl, which is essential to the ion exchange of methylene blue cations with H^+ions. According to findings from pH studies, the beta-CD@ML shows a decrease in MB adsorption under strongly acidic conditions. The carboxylate group was subsequently converted into a carboxylic acid (-COOH) through regeneration (Lagiewka et al., 2023). Various adsorbent characteristics were examined at the end of the fifth cycle to check the structural stability of beta-CD@ML in recovery cycles. Fig. 8(c) shows the FTIR spectrum of recovered beta-CD@ML with fresh samples. The peaks associated with different functional groups were visible in the recovered sample but with a lower intensity than in the fresh adsorbent sample, illustrating little changes in the chemical structure during the adsorption-desorption processes.

The saturation magnetization value of beta-CD@ML was initially measured 2.6 emu g^{-1}, but it decreased to 2.4 emu g^{-1} after five recovery cycles (Fig. 8(d)). A slight change in magnetic property was observed after five recovery steps, and the recovered beta-CD@ML demonstrated good separation by a magnetic field. In summary, FT-IR and VSM analyses confirmed the stability of beta-CD@ML throughout the adsorption-desorption processes and proved its reliability for practical applications.

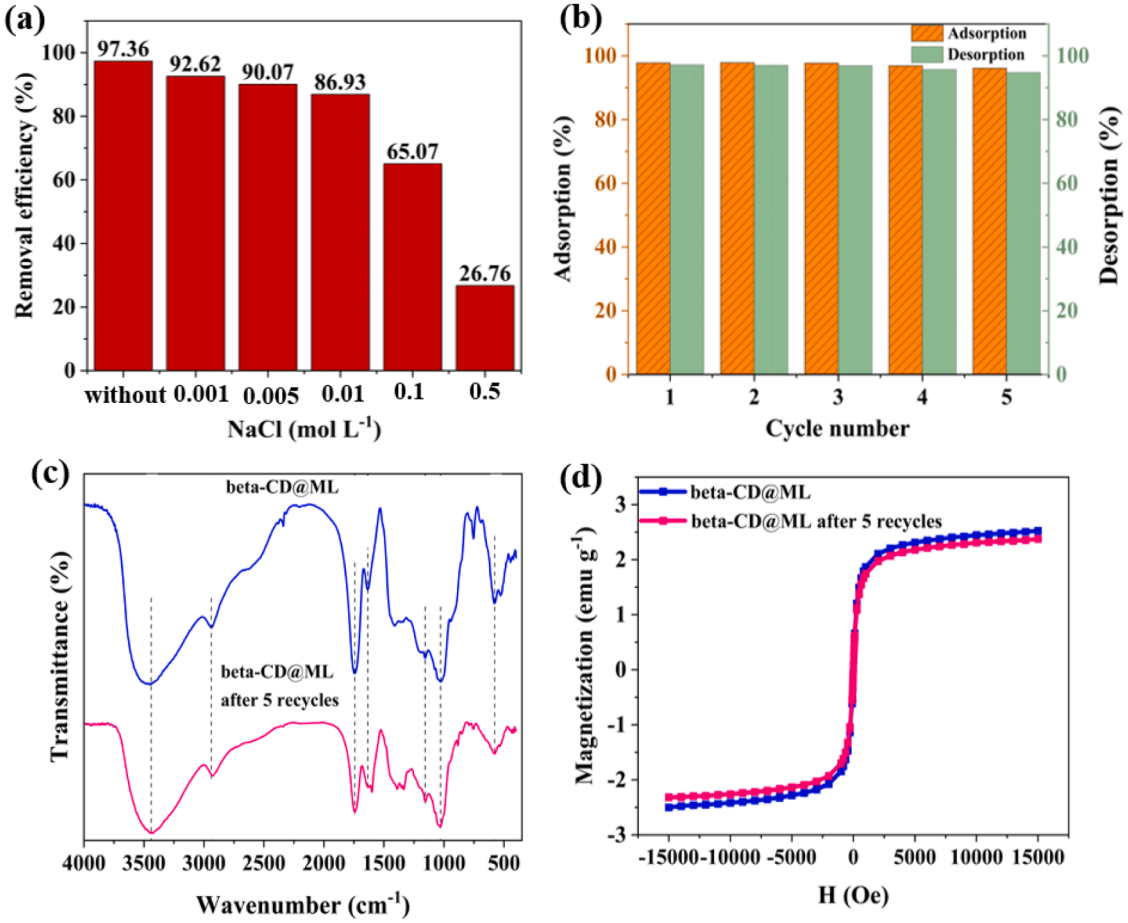

Fig. 8. (a) Correlation between ionic strength and MB removal efficiency, (b) adsorption-desorption cycle of MB on beta-CD@ML, (c) FT-IR spectra of the fresh and the fifth recovered beta-CD@ML samples, and (d) Hysteresis curves of the fresh and the fifth recovered beta-CD@ML samples.

3.7. Proposed adsorption mechanism

The proposed mechanism of MB adsorption on beta-CD@ML is presented in Fig. 9(a). The hydrophobic cavity of the beta-CD unit contains bridging oxygen and hydrogen atoms. The inclusion complexation effect allows an MB molecule to be trapped in the interior space of this cavity (Jiang et al., 2019). The carboxylate anion (-COO-) of citric acid (Huang et al., 2018) effectively adsorb the cationic MB dye through electrostatic attraction, highlighting the importance of electrostatic interactions in adsorption. Furthermore, electrostatic interaction occurs between the positively charged nitrogen atoms of a dye molecule and the hydroxyl groups of lignin (Budnyak et al., 2018). Hydrogen bonds with oxygen-containing functional groups of beta-CD (Lagiewka et al., 2023) and lignin, and π–π interactions between MB and lignin also contribute to adsorption (Budnyak et al., 2018).

The FTIR spectra (Fig. 9(b)) provided insights into the adsorption mechanism by investigating the involvement of functional groups. Distinct deviations and intensity reduction in the characteristic peaks of beta-CD@ML-MB functional groups, compared to beta-CD@ML, indicate changes during adsorption. The decrease in intensity of the peak at 3455 cm^{-1} after MB adsorption suggests that adsorption has implications for the O—H stretching of the hydroxyl groups and may also affect hydrogen bonding within the complex. The peak at 2939 cm^{-1} does not show significant change. Therefore, C—H bonds of alkyl groups of glucose units do not participate in adsorption (Lagiewka et al., 2023). The intensity of the peak at 1743 cm^{-1} decreases significantly after adsorption because the carboxylate group (C = O) of citric acid interacts with the cationic dye (Huang et al., 2018). Before adsorption, the peak at 1594 cm^{-1} of lignin overlaps with the strong bond at 1635 cm^{-1} of beta-CD. After adsorption, the intensity of the 1635 cm^{-1} peak decreases slightly, indicating a weak interaction between C–C and MB. The lignin peak also appears at 1594 cm^{-1}, indicating the π-π stacking effect between the diphenyl lignin and MB aromatic rings. However, the contribution of π electrons to MB binding is minimal because of their weaker strength compared to electrostatic interactions or hydrogen bonding.

After adsorption, the peaks at 1157 cm^{-1} and 1028 cm^{-1} are less intense and broad, indicating the interaction between the lignin C—OH group and beta-CD glucose rings with MB. The change in the intensity of the 1028 cm^{-1} peak after adsorption indicates that MB molecules can be inserted because of cyclodextrin cavities (Lagiewka et al., 2023).

3.8. Comparison with other adsorbents

The beta-CD@ML adsorbent demonstrates a q_{max} of 80 mg g^{-1} for MB adsorption. This q_{max} value indicates significant adsorption of MB dye. By comparing this adsorbent with other adsorbents listed in Table S7, cyclodextrin-containing adsorbents, including beta-CD@ML, tend to show high q_{max} values because different functional groups contribute to effective adsorption.

4. Conclusions

In summary, the present work suggests an eco-friendly method for

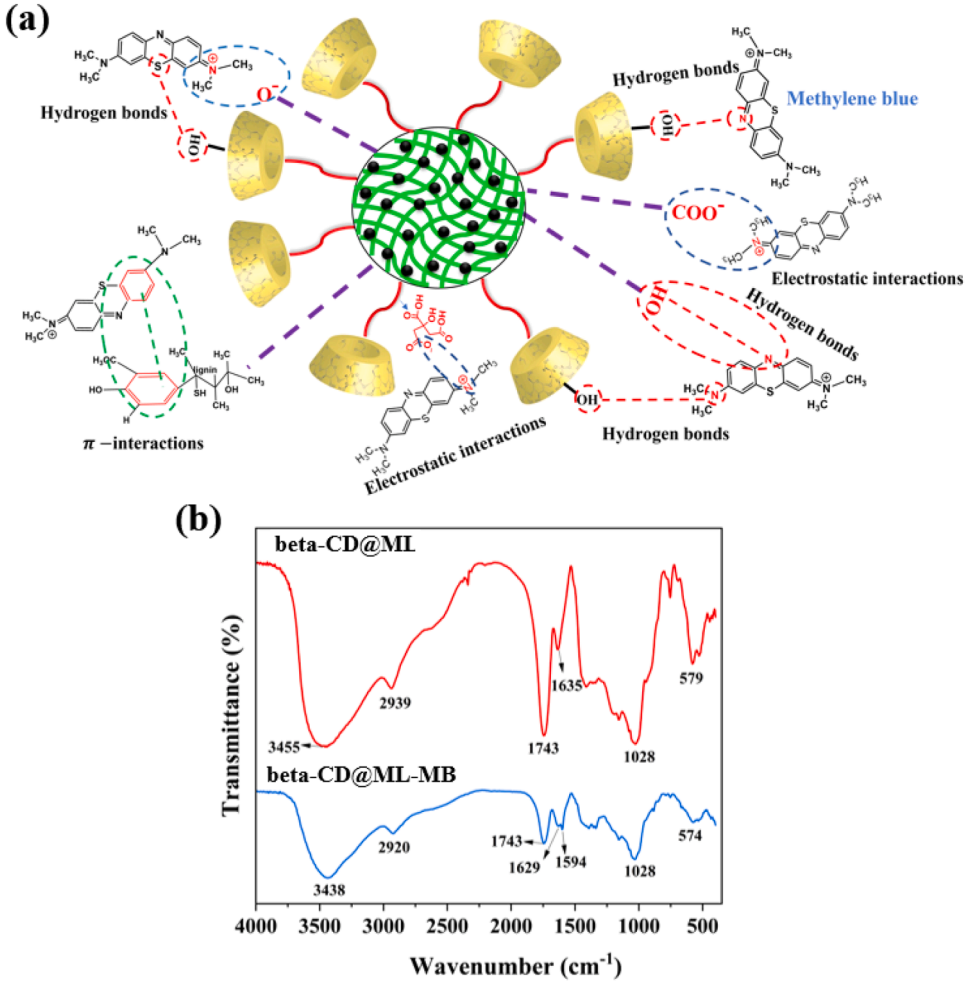

Fig. 9. (a) Adsorption mechanism of MB on beta-CD@ML, and (b) FT-IR spectra of fresh adsorbent and after MB adsorption.

preparing a multifunctional adsorbent (beta-CD@ML) using three safe and non-toxic materials, lignin, beta-cyclodextrin (beta-CD), and citric acid, then examining how well it works as an adsorbent for selective removal of cationic dyes. Various spectral methods were employed to characterize beta-CD@ML adsorbent. The adsorbent with a surface area of 5.37 $m^2\ g^{-1}$ showed a maximum adsorption capacity of 80 mg g^{-1} at 25 °C and achieved a high removal percentage of 97 % for methylene blue compared to magnetic lignin (55 %) under the same conditions. Therefore, with the structural analysis, the correctness of the adsorbent synthesis was confirmed, and the first hypothesis was confirmed by enhancing the removal of methylene blue for magnetic lignin after modifying it with beta-cyclodextrin. The PSO model and Langmuir isotherm provided the best fit among all models for the removal of methylene blue. Consequently, the adsorption process can be assigned to physical adsorption on a homogeneous surface. Thermodynamic analysis indicated that the adsorption is exothermic ($\triangle H^\circ > 0$) and is associated with a stochastic increase ($\triangle S^\circ > 0$). Electrostatic interaction, complexation, hydrogen bonding, and π-π stacking are the proposed mechanisms of interaction between beta-CD@ML and methylene blue during adsorption. The second hypothesis was confirmed due to the proof of different mechanisms in creating the interaction between adsorbent and methylene blue. The beta-CD@ML biosorbent exhibits promising potential for practical water treatment applications due to its facile synthesis, the use of a green and available cross-linker, magnetic properties for convenient recovery, good adsorption performance, and excellent regeneration capability.

CRediT authorship contribution statement

Arefe Moatamed Sabzevar: Writing – review & editing, Writing – original draft, Visualization, Methodology, Investigation, Formal analysis, Conceptualization. **Ali Ahmadpour:** Writing – review & editing, Validation, Supervision, Methodology, Funding acquisition, Data curation, Conceptualization. **Mahboube Ghahramaninezhad:** Writing – review & editing, Validation, Project administration, Methodology, Conceptualization.

Declaration of competing interest

The authors declare that they have no known competing financial interests or personal relationships that could have appeared to influence the work reported in this paper.

Acknowledgements

The authors appreciate the support of Ferdowsi University of Mashhad, Iran (Grant No. 61254) for this work.

Supplementary materials

Supplementary material associated with this article can be found, in the online version, at doi:10.1016/j.carpta.2024.100654.

Data availability

Data will be made available on request.

References

Ahmadpour, A., Tanhaei, B., Khoshkho, S. M., Ayati, A., Krivoshapkin, P., & Sillanpää, M. (2023). Dual-purpose magnetic κ-carrageenan/montmorillonite hydrogel for carrying and removal of tetracycline from aqueous medium. *Inorganic Chemistry Communications, 156*, 111274–111286. https://doi.org/10.1016/j.inoche.2023.111274

Amiri-Khamakani, Z., Salehi, M. M., Hassanzadeh-Afruzi, F., Mohammadi, M., Maleki, A., & Zare, E. N. (2024). Methyl alginate/Santa Barbara amorphous-15/iron oxide nanocomposite for efficient removal of different pollutants from aquatic environments. *Carbohydrate Polymer Technologies and Applications, 8*, 100562–100575. https://doi.org/10.1016/j.carpta.2024.100562

Amran, F., & Zaini, M. A. A. (2022). Beta-cyclodextrin adsorbents to remove water pollutants—A commentary. *Chemical Engineering Science, 16*, 1407–1423. https://doi.org/10.1007/s11705-022-2146-2

Budnyak, T. M., Aminzadeh, S., Pylypchuk, I. V., Sternik, D., Tertykh, V. A., Lindström, M. E., et al. (2018). Methylene Blue dye sorption by hybrid materials from technical lignins. *Journal of Environmental Chemical Engineering, 6*, 4997–5007. https://doi.org/10.1016/j.jtice.2016.06.009

Farooq, S., Xu, L., Ostovan, A., Qin, C., Liu, Y., Pan, Y., et al. (2023). Assessing the greenification potential of cyclodextrin-based molecularly imprinted polymers for pesticide detection. *Food Chemistry*, Article 136822.

Ge, Y., & Li, Z. (2018). Application of lignin and its derivatives in adsorption of heavy metal ions in water: A review. *ACS Sustainable Chemistry & Engineering, 6*, 7181–7192. https://doi.org/10.1021/acssuschemeng.8b01345

Ghahramaninezhad, M., & Ahmadpour, A. (2022). Carboxylmethyl-β-cyclodextrin as a good modifier agent for oxidation of dibenzothiophene. *Surfaces and Interfaces, 28*, 101612–101620. https://doi.org/10.1016/j.surfin.2021.101612

Han, Y., Ma, Z., Cong, H., Wang, Q., & Wang, X. (2022). Surface Chitosan-coated Fe_3O_4 immobilized lignin for adsorbed phosphate radicals in solution. *Biochemical Engineering Journal, 187*. https://doi.org/10.1016/j.bej.2022.108662, 108662-108629.

Hasan, M. J., Westphal, E., Chen, P., Saini, A., Chu, I.-W., Watzman, S. J., et al. (2023a). Adsorptive properties and on-demand magnetic response of lignin@Fe_3O_4 nanoparticles at castor oil–water interfaces. *RSC Advances, 13*, 2768–2779. https://doi.org/10.1039/D2RA07952F

Hasan, K., Shehadi, I. A., Joseph, R. G., Patole, S. P., & Elgamouz, A. (2023b). β-cyclodextrin-functionalized Fe3O4-supported Pd-nanocatalyst for the reduction of nitroarenes in water at mild conditions. *ACS Omega*, 23901–23912. https://doi.org/10.1021/acsomega.3c02332

Heravi, M., Srivastava, V., Ahmadpour, A., Zeynali, V., & Sillanpää, M. (2024). The effect of the number of SO_3^- groups on the adsorption of anionic dyes by the synthesized hydroxyapatite/Mg–Al LDH nanocomposite. *Environmental Science and Pollution Research International*, 1–22. https://doi.org/10.1007/s11356-024-32192-6

Huang, W., Hu, Y., Li, Y., Zhou, Y., Niu, D., Lei, Z., et al. (2018). Citric acid-crosslinked β-cyclodextrin for simultaneous removal of bisphenol A, methylene blue and copper: The roles of cavity and surface functional groups. *Journal of the Taiwan Institute of Chemical Engineers, 82*, 189–197. https://doi.org/10.1016/j.jtice.2017.11.021

Jiang, H.-L., Lin, J.-C., Hai, W., Tan, H.-W., Luo, Y.-W., Xie, X.-L., et al. (2019). A novel crosslinked β-cyclodextrin-based polymer for removing methylene blue from water with high efficiency. *Colloids and Surfaces A: Physicochemical and Engineering Aspects, 560*, 59–68. https://doi.org/10.1016/j.colsurfa.2018.10.004

Katahira, R., Elder, T. J., & Beckham, G. T. (2018). A brief introduction to lignin structure. In G. T Beckham (Ed.), *Lignin valorization: Emerging approaches* (pp. 1–20). Cambridge: RSC.

Khoshkho, S. M., Tanhaei, B., Ayati, A., & Kazemi, M. (2021). Preparation and characterization of ionic and non-ionic surfactants impregnated κ-carrageenan hydrogel beads for investigation of the adsorptive mechanism of cationic dye to develop for biomedical applications. *Journal of Molecular Liquids, 324*, 115118–115146. https://doi.org/10.1016/j.molliq.2020.115118

Kohzadi, H., & Soleiman-Beigi, M. (2021). XPS and structural studies of Fe_3O_4-PTMS-NAS@Cu as a novel magnetic natural asphalt base network and recoverable nanocatalyst for the synthesis of biaryl compounds. *Scientific Reports, 11*, 24508–24521. https://doi.org/10.1038/s41598-021-04111-z

Köse, K., Tüysüz, M., Aksüt, D., & Uzun, L. (2022). Modification of cyclodextrin and use in environmental applications. *Environmental Science and Pollution Research International, 29*, 182–209. https://doi.org/10.1007/s11356-021-15005-y

Lagiewka, J., Nowik-Zajac, A., Pajdak, A., & Zawierucha, I. (2023). A novel multifunctional β-cyclodextrin polymer as a promising sorbent for rapid removal of methylene blue from aqueous solutions. *Carbohydrate Polymers, 307*, 120615–120630. https://doi.org/10.1016/j.carbpol.2023.120615

Lee, S.-L., Park, J.-H., Kim, S.-H., Kang, S.-W., Cho, J.-S., Jeon, J.-R., et al. (2019). Sorption behavior of malachite green onto pristine lignin to evaluate the possibility as a dye adsorbent by lignin. *Applied Biological Chemistry, 62*, 1–10. https://doi.org/10.1186/s13765-019-0444-2

Li, Z., Xiao, D., Ge, Y., & Koehler, S. (2015). Surface-functionalized porous lignin for fast and efficient lead removal from aqueous solution. *Applied Materials & Interfaces, 7*, 15000–15009. https://doi.org/10.1021/acsami.5b03994

Liu, Q., Zhou, Y., Lu, J., & Zhou, Y. (2020). Novel cyclodextrin-based adsorbents for removing pollutants from wastewater: A critical review. *Chemosphere, 241*, 125043–125094. https://doi.org/10.1016/j.chemosphere.2019.125043

Liu, Q., Wang, J., Duan, C., Wang, T., & Zhou, Y. (2022). A novel cationic graphene modified cyclodextrin adsorbent with enhanced removal performance of organic micropollutants and high antibacterial activity. *Journal of Hazardous Materials, 426*, 128074–128085. https://doi.org/10.1016/j.jhazmat.2021.128074

Lu, H.-Y., Li, X.-F., Zhang, C.-Q., Li, W.-H., & Xu, D.-P. (2019). β-Cyclodextrin grafted on alkali lignin as a dispersant for coal water slurry. *Energy Sources, Part A: Recovery, Utilization, and Environmental Effects, 41*, 1716–1724. https://doi.org/10.1080/15567036.2018.1549146

Mosoarca, G., Popa, S., Vancea, C., Dan, M., & Boran, S. (2022). Removal of methylene blue from aqueous solutions using a new natural lignocellulosic adsorbent—Raspberry (Rubus idaeus) leaves powder. *Polymers, 14*, 1966–1982. https://doi.org/10.3390/polym14101966

Osman, A. I., El-Monaem, E. M. A., Elgarahy, A. M., Aniagor, C. O., Hosny, M., Farghali, M., et al. (2023). Methods to prepare biosorbents and magnetic sorbents for

water treatment: A review. *Environmental Chemistry Letters*, 1–62. https://doi.org/10.1007/s10311-023-01603-4

Peng, F.-Y., Wang, P.-W., Liao, W., & Yu, I.-S. (2021). Lignin Biopolymer for the synthesis of iron nanoparticles and the composite applied for the removal of methylene blue. *Polymers, 13*, 3847–3859. https://doi.org/10.3390/polym13213847

Petitjean, M., Lamberto, N., Zornoza, A., & Isasi, J. R. (2022). Green synthesis and chemometric characterization of hydrophobic xanthan matrices: Interactions with phenolic compounds. *Carbohydrate Polymers, 288*, 119387–119396. https://doi.org/10.1016/j.carbpol.2022.119387

Przybyla, M. A., Yilmaz, G., & Becer, C. R. (2020). Natural cyclodextrins and their derivatives for polymer synthesis. *Polymer Chemistry, 11*, 7582–7602. https://doi.org/10.1039/D0PY01464H

Qu, J. J., Dong, M., Wei, S., Meng, Q., Hu, L., Hu, Q., et al. (2020). Microwave-assisted one pot synthesis of β-cyclodextrin modified biochar for concurrent removal of Pb (II) and bisphenol a in water. *Carbohydrate Polymers, 250*, 117003–117014. https://doi.org/10.1016/j.carbpol.2020.117003

Rahman, N., & Raheem, A. (2023). Mechanistic investigation of levofloxacin adsorption on Fe(III)-tartaric acid/xanthan gum/graphene oxide/polyacrylamide hydrogel: Box-Behnken design and Taguchi method for optimization. *Journal of Industrial and Engineering Chemistry, 127*, 110–124. https://doi.org/10.1016/j.jiec.2023.06.044

Rius-Ayra, O., Biserova-Tahchieva, A., & Llorca-Isern, N. (2023). Removal of dyes, oils, alcohols, heavy metals and microplastics from water with superhydrophobic materials. *Chemosphere, 311*, 137148–137164.

Rout, D. R., Jena, H. M., Baigenzhenov, O., & Hosseini-Bandegharaei, A. (2023). Graphene-based materials for effective adsorption of organic and inorganic pollutants: A critical and comprehensive review. *The Science of the Total Environment, 863*, 160871–160893. https://doi.org/10.1016/j.scitotenv.2022.160871

Salazar, S., Yutronic, N., & Jara, P. (2020). Magnetic β-cyclodextrin nanosponges for potential application in the removal of the neonicotinoid dinotefuran from wastewater. *International Journal of Molecular Sciences, 21*, 4079–4091. https://doi.org/10.3390/ijms21114079

Saravanan, A., Kumar, P. S., Jeevanantham, S., Karishma, S., Tajsabreen, B., Yaashikaa, P., et al. (2021). Effective water/wastewater treatment methodologies for toxic pollutants removal: Processes and applications towards sustainable development. *Chemosphere, 280*, 130595–130609. https://doi.org/10.1016/j.chemosphere.2021.130595

Sharma, S., & Bhattacharya, A. (2017). Drinking water contamination and treatment techniques. *Applied Water Science, 7*, 1043–1067. https://doi.org/10.1007/s13201-016-0455-7

Soares, V., Moraes, A. F.d. S.d., Santos, J.d., Grando, M. C., Luz, C.d., Colpani, G. L., et al. (2019). Obtaining of Fe_3O_4@C core-shell nanoparticles as an adsorbent of tetracycline in aqueous solutions. *Materials Research, 22*, e20180857–e20180867. https://doi.org/10.1590/1980-5373-MR-2018-0857

Tang, P., Sun, Q., Zhao, L., Tang, Y., Liu, Y., Pu, H., et al. (2019). A simple and green method to construct cyclodextrin polymer for the effective and simultaneous estrogen pollutant and metal removal. *Chemical Engineering Journal, 366*, 598–607. https://doi.org/10.1016/j.cej.2019.02.117

Tanhaei, B., Ayati, A., Lahtinen, M., & Sillanpää, M. (2015). Preparation and characterization of a novel chitosan/Al_2O_3/magnetite nanoparticles composite adsorbent for kinetic, thermodynamic and isotherm studies of Methyl Orange adsorption. *Chemical Engineering Journal, 259*, 1–10. https://doi.org/10.1016/j.cej.2014.07.109

Varan, G., Varan, C., Erdoğar, N., Hıncal, A. A., & Bilensoy, E. (2017). Amphiphilic cyclodextrin nanoparticles. *International Journal of Pharmaceutics, 531*, 457–469. https://doi.org/10.1016/j.ijpharm.2017.06.010

Verma, M., Lee, I., Hong, Y., Kumar, V., & Kim, H. (2022). Multifunctional β-Cyclodextrin-EDTA-Chitosan polymer adsorbent synthesis for simultaneous removal of heavy metals and organic dyes from wastewater. *Environmental Pollution (Barking, Essex: 1987), 292*, 118447–118450. https://doi.org/10.1016/j.envpol.2021.118447

Waheed, A., Baig, N., Ullah, N., & Falath, W. (2021). Removal of hazardous dyes, toxic metal ions and organic pollutants from wastewater by using porous hyper-cross-linked polymeric materials: A review of recent advances. *Journal of Environmental Management, 287*, 112360–112380. https://doi.org/10.1016/j.jenvman.2021.112360

Wei, T., Wu, H., & Li, Z. (2023). Lignin immobilized cyclodextrin composite microspheres with multifunctionalized surface chemistry for non-competitive adsorption of co-existing endocrine disruptors in water. *Journal of Hazardous Materials, 441*, 129969–129980. https://doi.org/10.1016/j.jhazmat.2022.129969

Wu, H., Gong, L., Zhang, X., He, F., & Li, Z. (2021). Bifunctional porous polyethyleneimine-grafted lignin microspheres for efficient adsorption of 2, 4-dichlorophenoxyacetic acid over a wide pH range and controlled release. *Chemical Engineering Journal, 411*, 128539–128549. https://doi.org/10.1016/j.cej.2021.128539

Yang, Z., Zhang, X., Yao, X., Fang, Y., Chen, H., & Ji, H. (2016). β-cyclodextrin grafted on lignin as inverse phase transfer catalyst for the oxidation of benzyl alcohol in H_2O. *Tetrahedron, 72*, 1773–1781. https://doi.org/10.1016/j.tet.2016.02.036

Yatimzade, M. H., Ahmadpour, A., Ghahramaninezhad, M., & Sabzevar, A. M. (2024). Optimizing the efficient removal of ibuprofen from water environment by magnetic carbon aerogel: Kinetics, isotherms, and thermodynamic studies. *Journal of Molecular Liquids, 408*, 125337–125342. https://doi.org/10.1016/j.molliq.2024.125337

Zhang, J., Jiang, F., Lu, Y., Wei, S., Xu, H., Zhang, J., et al. (2023). Lignin microparticles-reinforced cellulose filter paper for simultaneous removal of emulsified oils and dyes. *International Journal of Biological Macromolecules, 230*, 123120–123132. https://doi.org/10.1016/j.ijbiomac.2022.123120

Zhou, Y., Hu, Y., Huang, W., Cheng, G., Cui, C., & Lu, J. (2018). A novel amphoteric β-cyclodextrin-based adsorbent for simultaneous removal of cationic/anionic dyes and bisphenol A. *Chemical Engineering Journal, 341*, 47–57. https://doi.org/10.1016/j.cej.2018.01.155